Pergamon

Int. J. Solids Structures Vol. 31, No. 8, pp. 1133–1148, 1994

0020–7683/94 $6.00 + .00

MODE II FRACTURE TOUGHNESS OF A BRITTLE ADHESIVE LAYER

Z. CEDRIC XIA and JOHN W. HUTCHINSON
Division of Applied Sciences, Harvard University, Cambridge, Mass. U.S.A.

(*Received* 31 *March* 1993; *in revised form* 14 *September* 1993)

Abstract—This paper concerns the analytical estimation of the macroscopic mode II fracture toughness of a brittle adhesive layer sandwiched between and bonding together stiff substrates. The process of failure involves the propagation and coalescence of microscopic tensile cracks ahead of the macroscropic mode II crack tip. The basic problem at the heart of the analysis is the plane strain problem for a layer subject to shear and containing a periodic array of micro-cracks which grow and coalesce under the condition that their tips advance under pure mode I conditions. A numerical solution to this basic problem is obtained and is then used to make detailed predictions for conditions for tunneling of the micro-cracks and for the evolution of their shape and spacing. These predictions are used in turn to develop the shearing traction–displacement relation for the brittle adhesive layer. The work per unit length of layer needed to drive the microcracks to coalescence can be identified with the macroscopic work of fracture in mode II, Γ_{IIc}, as is discussed via a cohesive zone model. The macroscopic model II toughness is predicted to be between three and four times the mode I fracture toughness, Γ_{Ic}, depending on constraints provided by substrates and very slightly on Poisson's ratio, ν. The theoretical predictions are compared with experimental data reported in the literature. Also discussed are the consequences of the assumption underlying the analysis that there exists an ample population of initial flaws whose largest dimension is roughly comparable to the thickness of the layer.

1. INTRODUCTION

Once initiated, cracks in homogeneous, isotropic brittle materials tend to advance under mode I conditions, assuming continuously applied loads. Thus, for example, when a crack propagates under plane strain conditions it selects a trajectory such that its mode II stress intensity factor, K_{II}, vanishes. This so-called "local symmetry" condition dictates many crack patterns found in brittle thin films or substrates where cracking occurs. Recent studies have detailed a number of interesting crack paths governed by this condition. Examples include studies of the development of wing cracks under compressive loading by Ashby and Hallam (1986) and by Horii and Nemat-Nasser (1986), of spiral cracking around a strained cylindrical inclusion by Freund and Kim (1991), and of cracking behavior due to localized hot shock of a brittle substrate by Tvergaard *et al.* (1993). The theoretical study most closely related to the present work is that of Fleck (1991) on the growth of periodic echelon cracks in an infinite substrate under combined shear and tensile loadings.

Macroscopic mode II crack growth is frequently observed in a very thin brittle adhesive layer which bonds together two substrates which confine the cracking process to the layer. If the crack does not follow one of the interfaces, one often observes scalloped fracture areas on the crack surface and many sigmoidal microcracks ahead of the main crack tip (see, for example, Hibbs and Bradley, 1987; Smith and Grove, 1987; Chai, 1988, and Fleck, 1992). Similar behavior takes in the matrix material between closely spaced parallel fibers in a composite. The fracture process seems to start with the initiation of sigmoidal tensile microcracks ahead of the crack tip and continue with the spreading of this damage leading to a distribution of microcracks such as that shown in Fig. 1(a). Macroscopic shear crack growth is initiated by coalescence of the main tip with the tensile microcracks just ahead of it. The experimentally measured work of fracture needed to advance such a mode II crack is found to be greater than the mode I work of fracture, with Γ_{IIc}/Γ_{Ic} ranging from 3 to 10 for brittle or moderately brittle materials (Hibbs and Bradley, 1987; Bradley, 1989, Fleck, 1992).

The aim of this study is the analytical estimation of macroscopic mode II fracture toughness of a brittle adhesive layer, Γ_{IIc}, in terms of the mode I toughness of the adhesive,

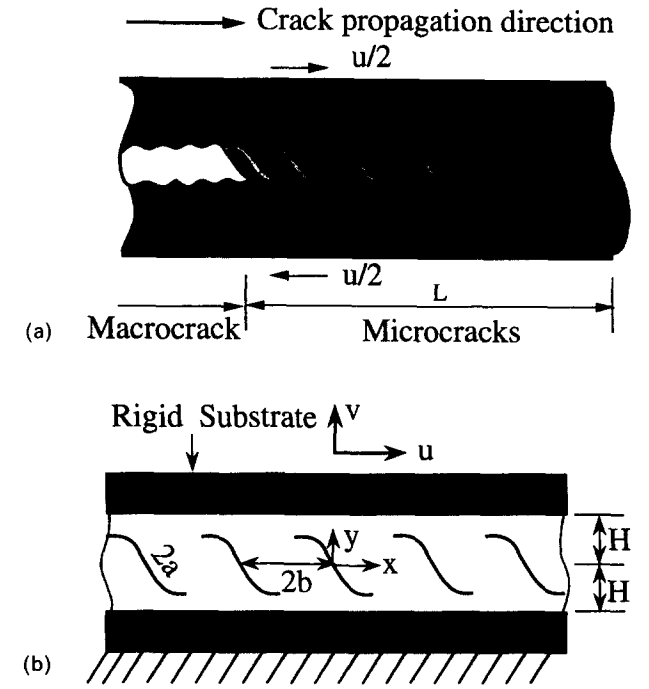

Fig. 1. (a) A schematic of the fracture process. (b) An array of curved tensile microcracks in the adhesive layer.

Γ_{Ic}. In mode I, the work of fracture of the sandwiched brittle layer *is* the mode I toughness of the adhesive, Γ_{Ic}, if the crack propagates in the interior of the layer and not along one of the interfaces between the adhesive and substrates (Fleck *et al.*, 1991). In developing the theoretical estimate of Γ_{IIc} it will be assumed that the spacing of the microcracks is small compared to the length of the zone of microcracking ahead of the macroscopic mode II crack. In effect, we work at two scales: the micro- and macroscales. On the microscale, we analyse the development of a periodic array of identical tensile microcracks, as shown in Fig. 1(b), and use these results to obtain a traction–displacement relation in shear, $\bar{\tau}(u)$, governing the macroscale behavior of the layer. A cohesive zone model of the mode II macrocrack is stipulated with $\bar{\tau}(u)$ as the shearing traction law in the cohesive zone ahead of the macrocrack. Well-known arguments employing the J-integral give the desired connection

$$\Gamma_{IIc} = \int_0^{u_c} \bar{\tau}(u)\, du, \tag{1}$$

where u_c is the shearing displacement at which the periodic microcracks coalesce and $\bar{\tau}$ drops to zero. The present study is the mode II counterpart to the modeling conducted by Ortiz (1988) of the effect of microcracks ahead of a mode I macrocrack.

The sections of the paper leading to explicit results from eqn (1) are organized as follows. Section 2 provides the solution to the basic plane strain problem shown in Fig. 1(b) for a periodic array of curved cracks, in a layer subject to remote shear loading, growing and coalescing under the condition that the mode II stress intensity factors at each crack tip vanish. Three quantities from this solution are needed to carry out the computation of $\bar{\tau}(u)$ and the prediction of Γ_{IIc}: the energy release rate for the in-plane growth of the plane strain cracks, G_{ps}; the effective in-plane shear modulus $\bar{\mu}$ of the cracked layer; and the energy release rate, G_{ss}, for each of the cracks when they tunnel in a direction perpendicular to the trace plane shown in Fig. 1(b). Complete results for these quantities are given in Section 2. The shearing traction–displacement relation, $\bar{\tau}(u)$, is derived in Section 3. This derivation has two steps. First, the evolution of the cracks' length and density as a

function of u is obtained using the basic results of Section 2. This step involves arguments as to when the microcracks will advance in their plane and when they will tunnel. It also involves the assumption that there exists a population of relatively large initial flaws in the adhesive from which the microcracks develop. Then, with the evolution of the length, shape and density of the cracks in hand, the traction–displacement law can be obtained from the results for $\bar{\mu}$. The final results for Γ_{IIc} are discussed in Section 4, along with a discussion of the implications of the assumption concerning the initial flaw population. Experimental observations which have been reported in the literature for mode II behavior of brittle adhesive layers are compared with the theory in this final section.

2. A PERIODIC ARRAY OF MODE I CRACKS IN A BRITTLE ADHESIVE LAYER SUBJECT TO SHEAR

2.1. *The plane strain problem*

The plane strain problem is introduced in Fig. 1(b). An adhesive layer of thickness $2H$ joins two substrates, It is often the case that the substrates are much stiffer than the adhesive. For the purpose of reducing the number of parameters in the problem and to simplify the analysis somewhat, we shall regard the substrates as two rigid grips perfectly bonded at each interface to the adhesive. The adhesive is taken to be isotropic, homogeneous and linearly elastic, with shear modulus, μ, and Poisson's ratio, ν. The external loading is applied through prescribed relative translations, u and v, of the two rigid grips. Two limiting shear loading cases are analysed corresponding to different constraints in the vertical direction. For a given prescribed tangential displacement u, either: (1) the grips are allowed to move freely in the vertical direction (i.e., the average normal traction exerted on the grips is zero), or (2) the grips are totally clamped in the vertical direction (i.e., $v = 0$).

The spacing separating the periodically distributed cracks in Fig. 1(b) is taken as $2b$, and the curvilinear length of each crack in the current state is denoted by $2a$. The solution procedure adopted in this study is that of representing the cracks as superposition of continuously distributed dislocations chosen to cancel the tractions on the crack surfaces via solution of coupled integral equations. The solution of a period array of dislocations in an elastic layer between rigid substrates is given in the Appendix. The outline of the setup of the integral equations and the numerical procedure for solving them can be found in Tvergaard *et al.* (1993). The procedure for advancing the crack tips such that pure mode I conditions always prevail at the tips is the same as that employed by Fleck (1991). It is this part of the solution method which determines the shape of the evolving cracks, as is now further described.

The process is started with an array of very short straight cracks with spacing $2b$ and inclined at 45° to the x-axis such that they are normal to the maximum principal stress of the uncracked layer. Since the cracks are very small initially, they behave almost like isolated cracks subject to tension perpendicular to their plane, and thus can be regarded as pure mode I cracks. The method for generating the subsequent crack trajectories is as follows. With the crack at its current length having $K_{II} = 0$, then the crack length is increased with the curvature of the next increment chosen such that the advanced tip is also in a state of pure mode I. More details of calculation procedure can be found in Fleck (1991). The plane strain energy release rate at the crack tips, G_{ps}, is related to the mode I stress intensity factor by the standard relation; the stress intensity factor is computed directly as the amplitude of the inverse square root singularity of the dislocation distribution at the ends of the crack.

When there are no cracks presented in the adhesive layer, the stress field is simply

$$\tau = \mu \frac{u}{2H} \tag{2}$$

and all other components are zero. After introduction of the periodic array of cracks, the average shear traction exerted at grips for a prescribed u is reduced below the value given

by eqn (2) and is denoted by $\bar{\tau}$. The effective shear modulus of the adhesive is denoted by $\bar{\mu}$ and is defined as

$$\bar{\mu} = \bar{\tau}\frac{2H}{u}. \tag{3}$$

The effective shear modulus is an important property which indicates the damage to the shear strength of the adhesive layer when cracks are present. Its primary purpose in the present paper will be to generate the traction–displacement relation $\bar{\tau}(u)$.

For a given crack shape, $\bar{\mu}$ is a function of the crack length/spacing ratio, a/b, the crack density ratio, H/b, and which of the two normal constraint conditions is imposed. This functional dependence can be determined from a direct computation of the average shear traction $\bar{\tau}$ when a value of u is prescribed, or it can be computed using a basic connection between compliance change and energy release rate derived as follows. Let s be the length of the evolving curved crack which started with length 0 and has grown to its current length $2a$. The elastic strain energy U stored in the layer per crack (with spacing $2b$) is

$$U = \tfrac{1}{2}\bar{\tau}u2b = \frac{u^2 b}{2H}\bar{\mu}. \tag{4}$$

The plane strain energy release rate G_{ps} at each tip at the current crack length $2a$ is given by

$$G_{ps}(a) = -\frac{1}{2}\frac{\partial U(a)}{\partial a}. \tag{5}$$

The combination of eqns (4) and (5) gives, together with the initial condition $\bar{\mu} = \mu$ when $s = 0$

$$\bar{\mu}(a) = \mu - \frac{4H}{u^2 b}\int_0^a G_{ps}(s)\,\mathrm{d}s. \tag{6}$$

As the crack length $2a$ approaches the critical length $2a_c$ where the cracks coalesce, the effective modulus $\bar{\mu}$ must approach zero. This fact provides an additional consistency check on the accuracy of the numerical calculations.

The numerical results for G_{ps}, $\bar{\mu}$ and for the shapes of the crack trajectories are shown in Figs 2–4 and will be explained in detail. The boundary-value problems have displacement-type conditions along the grip interfaces, and therefore the solutions do depend on Poisson's ratio. The results shown in these figures were computed with $\nu = 1/3$, but selected numerical checks indicated there is little dependence on ν for the normalized quantities employed. Recall that the solution process starts with a prescribed value of crack density H/b and with very short straight cracks oriented at 45° to the centerline of the layer. The cracks are then advanced under pure mode I conditions. Two distinct behaviors are found, unlike the shapes discovered by Fleck (1991), who considered an infinitely thick layer subject to combinations of shear and normal loading. In the case of the layer which has zero average normal traction, it is found that the cracks grow toward the interfaces of the adhesive and the rigid grips when the crack density, H/b, is less than about 0.81 with final shapes typical of those shown in the insert of Fig. 2(a). For crack densities, H/b, greater than 0.81 the cracks do not impinge upon the rigid grips but instead turn toward their neighbors and coalesce, as shown in the inserts in Figs 2(b) and (c), (here, again, the complete crack trajectories are shown). In the regime where the cracks coalesce, the shapes are relatively independent of H/b and the pattern scales with the spacing b. This limiting behavior would have been more evident had G_{ps} been normalized by b rather than H in the ordinate of Figs 2(b) and (c). (The choice of H rather than b for the normalization facilitates application of the results discussed later.) When H/b is large, the present results agree with those of

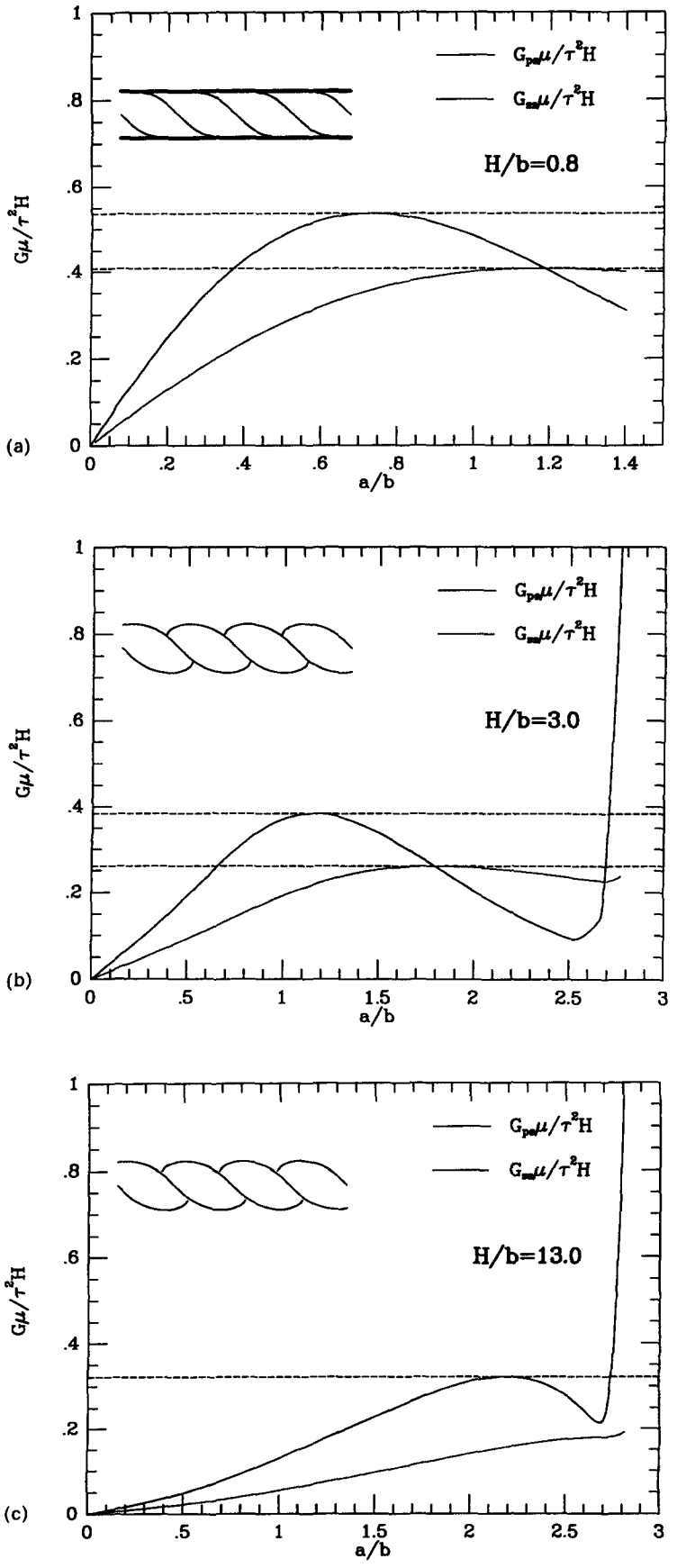

Fig. 2. Normalized G_{ps} and G_{ss} for three typical crack density parameter H/b and corresponding crack trajectories. (a) $H/b = 0.80$, (b) $H/b = 3.0$, (c) $H/b = 13.0$.

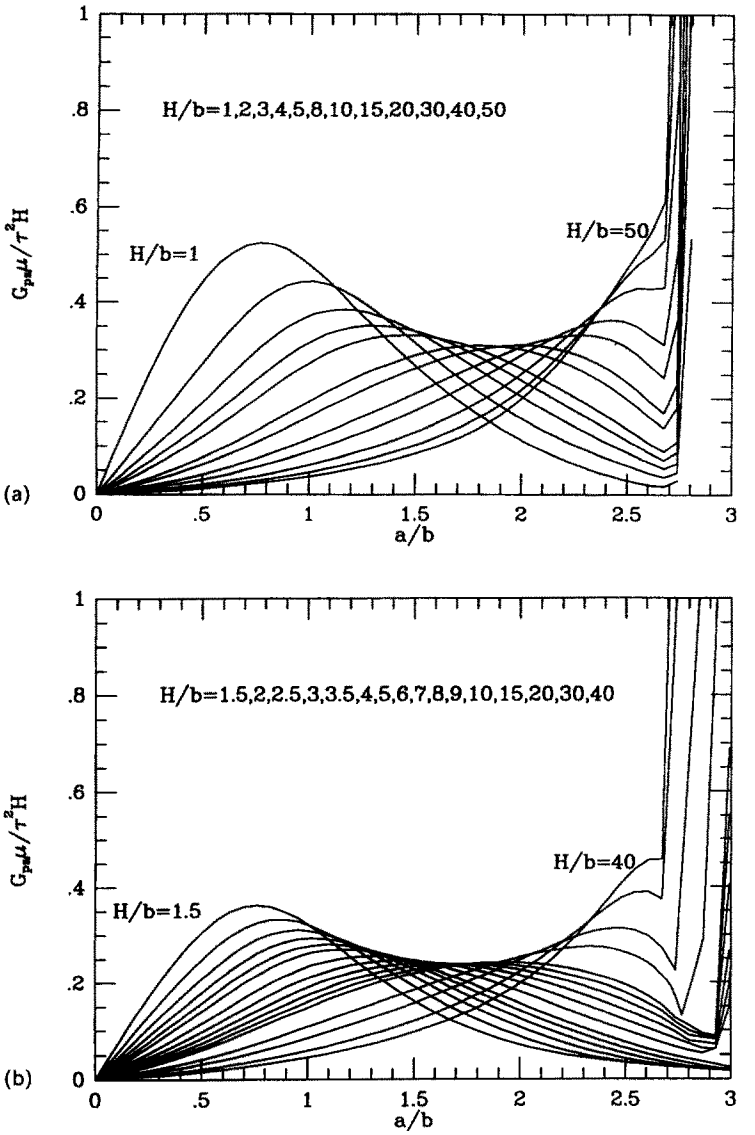

Fig. 3. Normalized G_{ps} for various crack density parameter H/b. (a) For zero average normal traction constraint. (b) For zero normal displacement constraint.

Fleck (1991) for echelon crack arrays in an infinitely thick slab. The transition in shapes in the second case, where the normal separation of the rigid grips is constrained to be zero, occurs at about $H/b = 2.6$. The three parts of Fig. 2 display the dependence of the normalized G_{ps} on the crack length/spacing ratio, a/b, for the three values of the crack density parameter H/b, all for the case of no average normal traction. An important feature of this dependence is the existence of a local maximum in the normalized energy release rate which is attained when the cracks are still well away from coalescence. In the regime where the cracks coalesce, the normalized G_{ps} becomes unbounded as the tips approach the crack surface of their neighbor. It is again worth emphasizing, the trajectories shown are pure mode I trajectories, and at no point as the cracks are advanced do opposite points on the crack faces come into contact (i.e., the cracks are fully open). Figure 2 also contains results for the tunneling energy release rate, G_{ss}, which will be introduced in the next subsection.

The complete results for the normalized plane strain energy release rate are plotted in Fig. 3 for the entire range of H/b needed in the present study for each of the two limiting normal constraint cases. The companion curves for the normalized effective shear modulus of the layer, $\bar{\mu}/\mu$, are shown in Fig. 4.

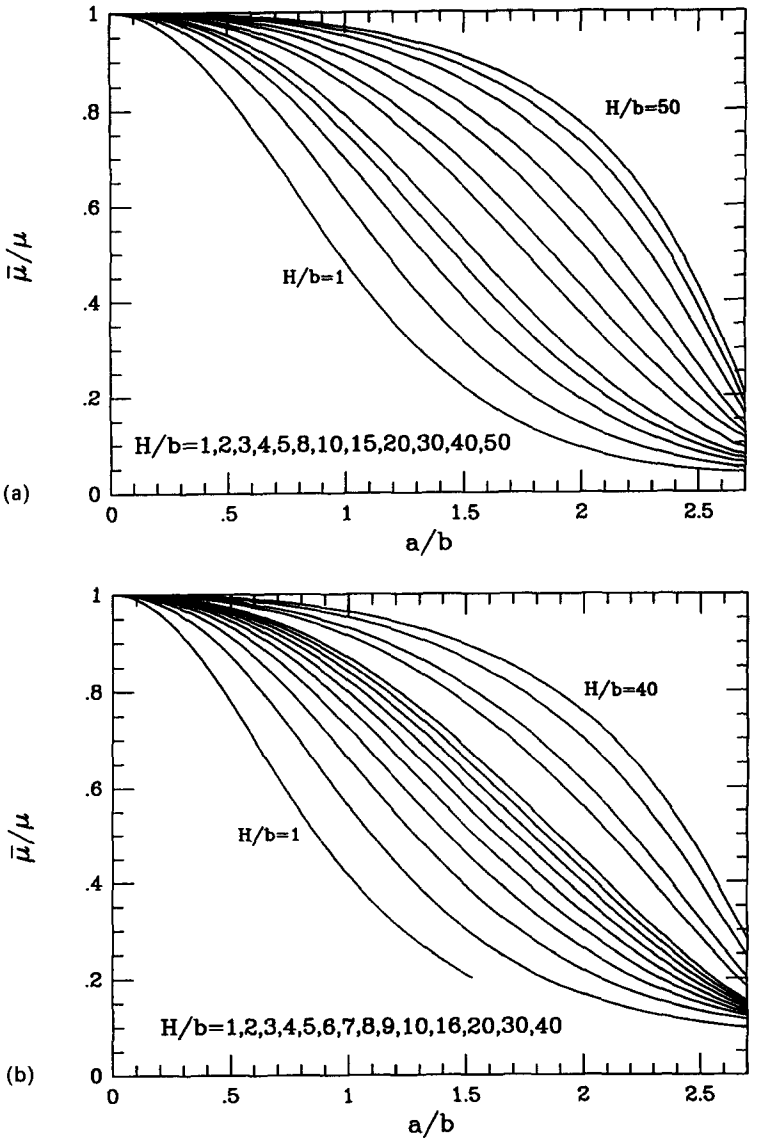

Fig. 4. Normalized effective shear modulus $\bar{\mu}$. (a) For zero average normal traction constraint. (b) For zero normal displacement constraint.

2.2. *Steady-state tunneling cracks and evaluation of* G_{ss}

Crack nucleation and growth in an adhesive layer is a very complicated process. It is a full three-dimensional (3D) problem in the sense that cracks will initiate from an existing population of flaws and propagate both in the plane [i.e., in the (x, y) plane of Fig. 1] and out of the plane (i.e., the z-direction in Fig. 1). Extensive propagation out of the plane is referred to as tunnel cracking. This is a form of cracking which is very common in thin brittle films and layers (Hutchinson and Suo, 1991; Beuth, 1992; Ye *et al.*, 1992; Ho and Suo, 1993). It is the primary mechanism by which roughly equiaxed initial flaws become greatly extended cracks in the tunneling direction. This mechanism is clearly expected to play a dominant role in establishing cracks in the brittle shear layer which are very long in the out-of-plane direction compared to their in-plane length, i.e., essentially plane strain cracks. In steady-state, the crack propagates in the out-of-plane direction at constant applied load with the tunnel front maintaining its shape as it advances. The steady-state energy release rate, G_{ss}, no longer depends on the tunneling length, nor on the initial flaw geometry.

The steady-state energy release rate G_{ss} along the tunneling front can be computed using quantities from the 2D plane strain crack solution without resorting to a 3D analysis.

Since the energy released per unit length of tunneling in the z-direction equals the energy released to form the plane strain crack traversing the layer (on a per crack basis), it readily follows that (e.g., Hutchinson and Suo, 1991)

$$G_{ss}(a) = \frac{1}{a}\int_0^a G_{ps}(s)\,\mathrm{d}s. \tag{7}$$

This is the relation which is used here to compute G_{ss}. An additional interesting relation between G_{ss} and G_{ps} noted by Beuth (1992), which will be of use later, is obtained by taking the derivative of eqn (7) with respect to a

$$\frac{\mathrm{d}G_{ss}}{\mathrm{d}a} = \frac{1}{a}(G_{ps} - G_{ss}). \tag{8}$$

Thus $G_{ss} = G_{ps}$ defines a condition at which G_{ss} achieves a local maximum with respect to in-plane crack length.

Numerical results for G_{ss} can be generated using eqn (7) and the results of Figs 2 and 3. The three plots of Fig. 2 include curves of normalized G_{ss} illustrating the trends and the fact expressed by eqn (8) that the maximum of G_{ss} at a prescribed u occurs where the two energy release rates are equal. Note that G_{ss} exceeds G_{ps} at crack lengths larger than those at the crossover point so that the crack driving force for tunneling will exceed that for in-plane extension in that regime. The results shown apply to a family of identical cracks spaced a distance $2b$ apart, all tunneling together as illustrated in Fig. 5(a). We now take

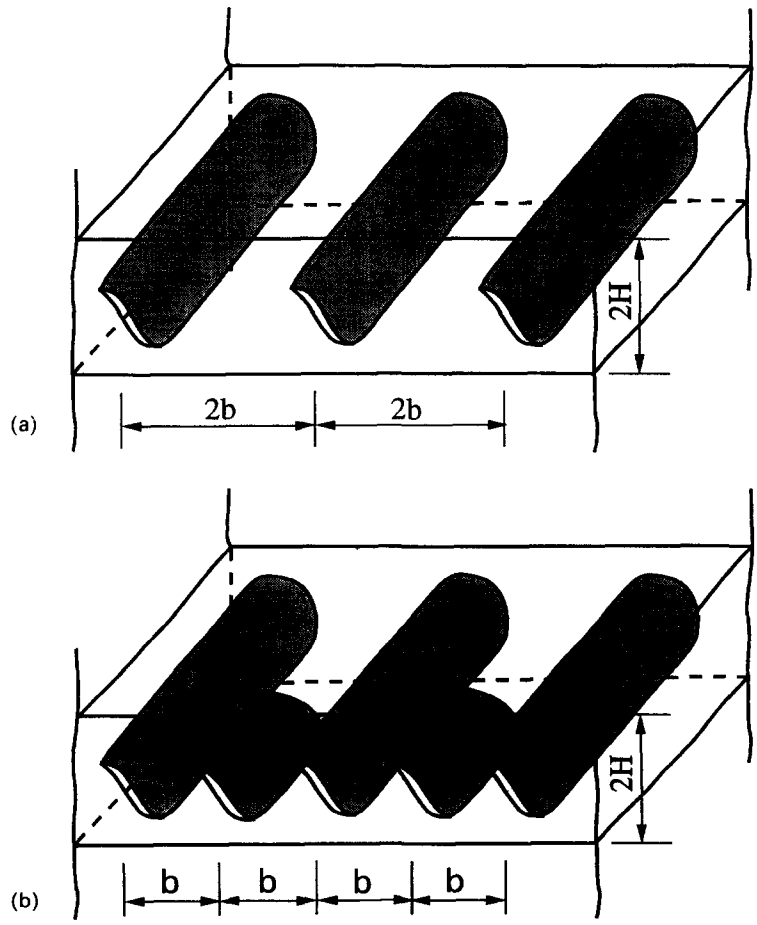

Fig. 5. (a) A set of tunneling cracks with spacing $2b$ in the adhesive layer. (b) A new set of tunneling cracks bisecting a pre-existing set of fully tunneled cracks.

one further step and derive the steady-state energy release rate for a new set of tunnel cracks of identical cross-sectional shape which precisely bisect a pre-existing set of fully tunneled cracks, as depicted in Fig. 5(b). The steady-state energy release rate for this new set of cracks is denoted by $\hat{G}_{ss}$.

2.3. $\hat{G}_{ss}$ *for sequential tunnel cracking*

Consider now the derivation of the steady-state energy release rate for the sequential cracking process shown in Fig. 5(b), where a set of new cracks of spacing $2b$ tunnels, precisely bisects a pre-existing set of spacing $2b$. Let $G_{ss}(b)$ denote the result of Section 2.2 for tunnel cracks of spacing b and let $G_{ss}(2b)$ be the result for spacing $2b$, both for the same prescribed value of u. Let $\hat{G}_{ss}$ be the energy release rate for the new set of tunneling cracks. Following the argument given by Hutchinson and Suo (1991), one has precisely

$$\hat{G}_{ss}(b) = 2G_{ss}(b) - G_{ss}(2b) \tag{9}$$

stating that the energy released by each new crack is the difference between the down-stream rate (for two cracks per new crack) and the up-stream rate. Thus, the steady-state energy release rate for the sequential process can also be obtained from the results for G_{ps} using eqns (7) and (9). Curves of normalized $\hat{G}_{ss}$ as a function of a/b are plotted in Fig. 6 for various H/b for the two constraint cases. Note that these results apply to a new set with spacing $2b$ tunneling between an existing set of spacing $2b$, i.e. the situation depicted in Fig. 5(b). In Section 3, results for $\hat{G}_{ss}$ and G_{ps} will be used in an approximate way to predict the evolution of both the spacing and lengths of the cracks in the layer as a function of u.

3. CRACK SPACING AND $\bar{\tau}(u)$

As a crack grows from an initial flaw in a brittle isotropic material comprising the layer, its crack front adjusts to a curved shape such that at every point it is in mode I with its energy release rate equal to the mode I toughness of the material, Γ_{Ic}. Once it has tunneled a distance of about two times its in-plane length the crack rapidly approaches the asymptotic steady-state condition analysed for periodically spaced cracks in the previous section. Crack propagation is entirely in the out-of-plane direction, advancing under constant applied shear displacement u and leaving behind an in-plane crack of fixed shape and length. A rigorous analysis of this three dimensional process is extremely difficult and is not attempted for the present shear layer problem. [A 3D analysis has been carried out for a thin film cracking problem by Nakamura and Kamath (1992) demonstrating for that problem that steady-state conditions are essentially attained once the crack has grown to a length of about twice the film thickness.] As noted in the discussion of Fig. 2, except for very high crack densities, there is a range of a/b in which G_{ss} exceeds G_{ps}. This implies that the 3D process of growth from a roughly equiaxed initial crack-like flaw will involve both in-plane and out-of-plane growth until the crack reaches the point where out-of-plane tunneling is favoured. Once steady-state is achieved, tunneling will be completed in the out-of-plane direction resulting in a set of plane strain cracks. Then, as u is further increased, these cracks will undergo further in-plane extension until conditions are met for a new set of cracks to begin tunneling between the present set. An approximate analysis of this sequential process is now given.

3.1. *Evolution of crack density as a function of* u

Suppose a periodic array of fully tunneled plane strain cracks exists with spacing $2b$. The condition for a new set to tunnel between the existing set as depicted in Fig. 5(b) is obtained as follows. When u reaches the level corresponding to $\hat{G}_{ss}(b) = \Gamma_{Ic}$, steady-state tunneling of the new set can occur with the outcome being a set of fully tunneled plane strain cracks of spacing b. Setting $\hat{G}_{ss}(b) = \Gamma_{Ic}$ and plotting the result in the form of $u\sqrt{\mu/(\Gamma_{Ic}H)}$ as a function of a/b for fixed values of H/b leads to curves such as those in Fig. 7. Note that for a given value of spacing $2b$ (i.e. a given value of H/b), there is a minimum value of u below which a set of new cracks cannot tunnel. If it is assumed that

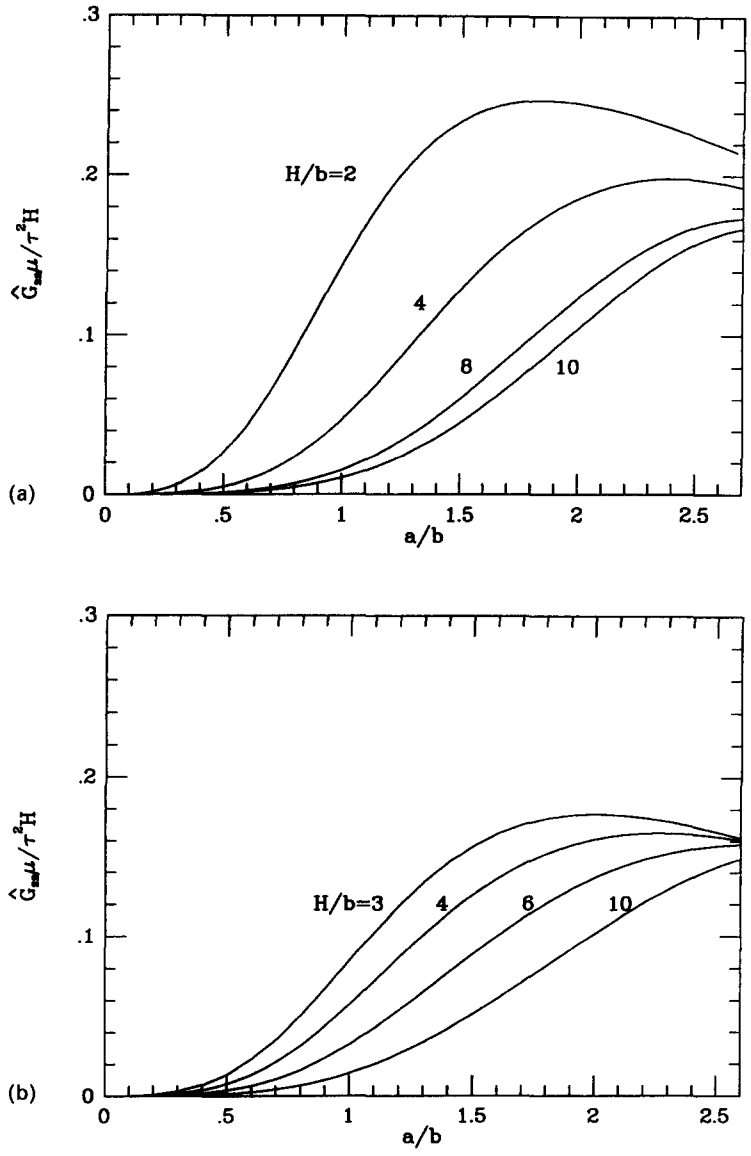

Fig. 6. Normalized $\hat{G}_{ss}$ as a function of a/b for various H/b (cf. Fig. 5b). (a) For zero average normal traction constraint. (b) For zero normal displacement constraint.

the initial flaw population is sufficiently large and plentiful such that the new set will initiate and tunnel when u reaches the minimum in Fig. 7 for the given H/b, then the crack spacing history lies along the trajectory of minima in Fig. 7. Given some initial spacing $2b_0$, say, then the subsequent spacings must be b_0, $b_0/2$, $b_0/4$, etc., for the sequential process envisioned, but a strict adherence to this sequence can be relaxed as described later. Figure 8 displays the crack density parameter H/b determined as just outlined as a function of the normalized u for each of the two constraint cases. The threshold values correspond to the minimum values of normalized u where tunneling of isolated cracks can first occur. The crack density increases from zero to a very high density (e.g., H/b = 5–10) over a relatively small range of u, corresponding to roughly only a 75% increase above threshold. Each curve in Fig. 8 is terminated with a horizontal dashed line at the crack density where the tunneling energy release rate no longer exceeds the plane strain release rate at any crack length a (cf. of Fig. 2c). Exactly how new cracks develop in this regime is not clear, but tunneling is not expected. In any case, by the point where the crack density reaches these levels, all the important contributions to the macroscopic toughness have been made.

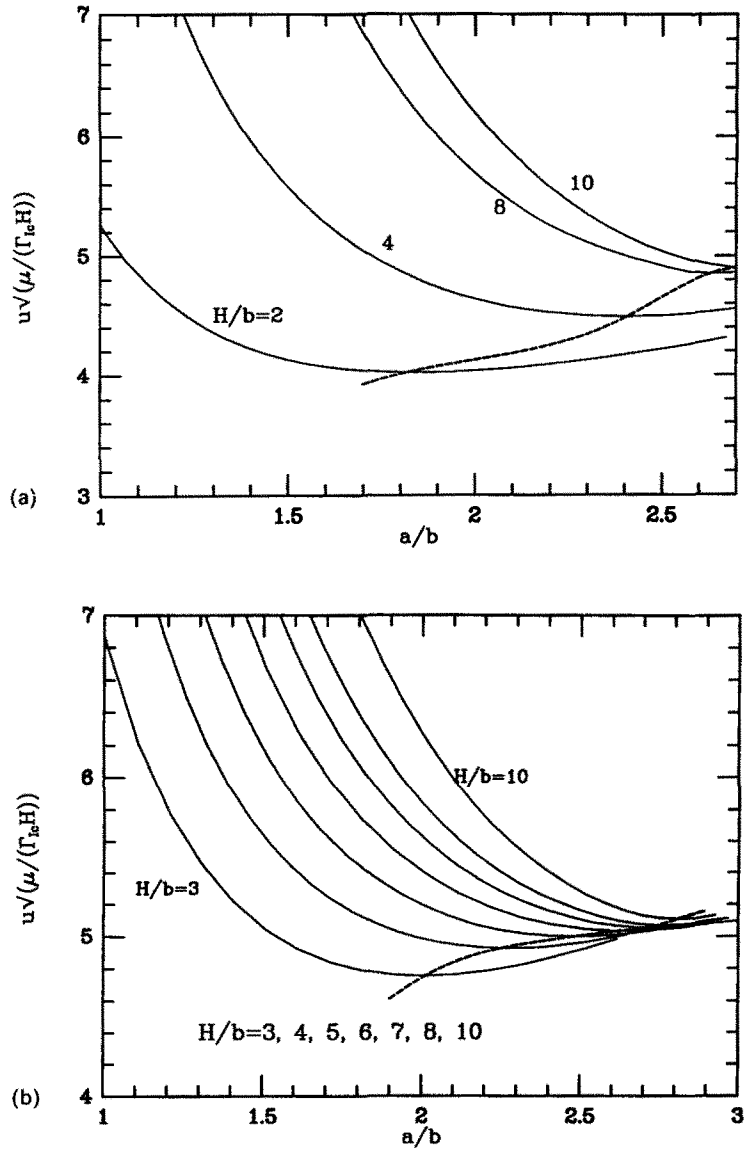

Fig. 7. Normalized u as a function of a/b with $\hat{G}_{ss}$ identified as Γ_{Ic}. (a) For zero average normal traction constraint. (b) For zero normal displacement constraint.

3.2. *Traction–displacement relation in shear*, $\bar{\tau}(u)$

With the relation between H/b and u in hand, it is possible to generate the desired relation $\bar{\tau}(u)$ in the following straightforward manner. For a prescribed value of u, obtain H/b from Fig. 8. This value characterizes the current spacing of the plane strain cracks. The in-plane length a of these cracks is then obtained from the ratio a/b using the results in Fig. 7. Once a/b is known, use the curves of Fig. 4 to obtain $\bar{\mu}/\mu$. Then, by eqn (3)

$$\bar{\tau}\sqrt{\frac{H}{\Gamma_{Ic}\mu}} = \frac{1}{2}\frac{\bar{\mu}}{\mu}u\sqrt{\frac{\mu}{\Gamma_{Ic}H}} \tag{10}$$

and it is this relation which is plotted for each of the constraint cases in Fig. 9. The peak values in Fig. 9 are associated with the onset of tunneling of widely spaced microcracks. The steep segments of the curves dropping from the peaks correspond to the range in which relatively widely spaced cracks tunnel with the sequential process of new sets tunneling and bisection existing sets. The steep portions end when the crack density reaches about $H/b = 2$

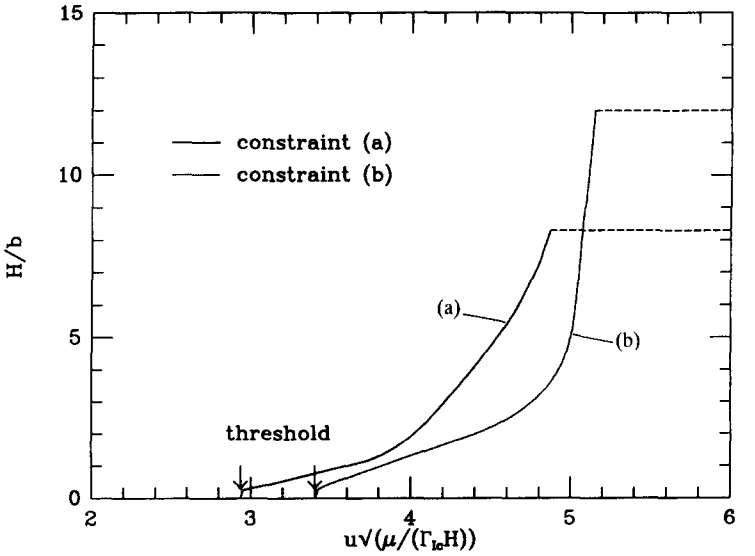

Fig. 8. Evolution of crack density H/b as a function of u.

for the case of zero average normal traction and at about $H/b = 3$ for the case of zero normal displacement. At higher densities the interaction between the cracks becomes dominant and $\bar{\tau}$ falls gradually with increasing u. The curves are terminated at the points labeled by $(u_c, \bar{\tau}_c)$ beyond which higher densities of tunneling cracks will not occur, i.e., at the density cutoffs indicated in Fig. 8.

Strictly speaking, the construction of the relation between $\bar{\tau}$ and u described above should start with some initial wide spacing $2b_0$ and then faithfully bisect the spacing according to the discrete values b_0, $b_0/2$, etc., leading to curves in Fig. 9 which would be segmented. The curves in Fig. 9 are generated by applying the calculation described above continuously as a function of u, ignoring the discrete nature of the sequential bisection process. The difference between the curves thus obtained and any segmented curve generated using some initial wide spacing $2b_0$ is not appreciable. The procedure described above approximates the actual cracking process in another sense. The shape of the cracks in the (x, y) plane depends on the crack density H/b. Thus, in any actual process the shapes of cracks which tunnel at one value of u will differ from those tunneling at another value of

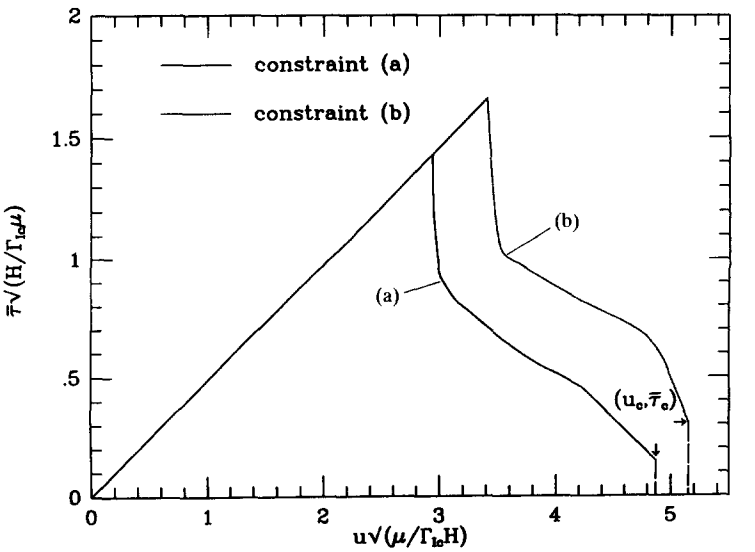

Fig. 9. The shearing traction–displacement relation $\bar{\tau}(u)$.

u. The procedure used here takes the *shapes* of all the cracks to be the same and to be that shape associated with the current value of u.

4. MACROSCOPIC MODE II TOUGHNESS, Γ_{IIc}

The results in Fig. 9 for $\bar{\tau}(u)$ enable one to calculate Γ_{IIc} using eqn (1). The final tail of $\bar{\tau}(u)$ has not been determined, and we neglect a small contribution to the integral in eqn (1) by terminating the integration at u_c as taken in Fig. 9. The results of the integration are

$$\Gamma_{IIc} = 3.1\Gamma_{Ic} \quad \text{for zero average normal traction}$$

$$\Gamma_{IIc} = 4.2\Gamma_{Ic} \quad \text{for zero normal displacement.}$$

The numerical results in this paper have all been calculated with a Poisson's ratio of 1/3, but, as mentioned earlier, the results are only weakly dependent on ν.

The present results are corroborated by Fleck's (1991) result, $\Gamma_{IIc} = 2.7\Gamma_{Ic}$, obtained for a single array of periodically spaced, tensile plane strain microcracks in an infinite solid subject to pure shear at infinity. This result represents the work of fracture per unit area needed to drive the sigmoidal echelon cracks to coalescence. More work is absorbed in the process envisioned in the present paper because of the influence of the constraint of the substrates and the fact that new cracks initiate and tunnel between existing cracks as u is increased. Nevertheless, the fact that the two analyses give results which are not significantly different suggests that the sequential details of the microcracking process may play a secondary role.

The cohesive zone model on which the above results are based can also be used to calculate the length of the cohesive zone L (see Fig. 1a) in which the "microscopic" traction–displacement relation $\bar{\tau}(u)$ holds. We have not computed L for the precise relation $\bar{\tau}(u)$ of Fig. 9, but a rough estimate indicates that it is on the order of H. Thus, the extent of the microcracking zone ahead of the macroscopic crack tip is only on the order of the most widely spaced cracks which make a significant contribution in the analysis leading to $\bar{\tau}(u)$, i.e., $b \cong H$. This suggests that an analysis which accounts for the interaction between the macrocrack and the individual microcracks in a discrete manner may give somewhat different predictions. Further work along these lines may be needed, especially if initiation from smaller flaws is considered important, as will be discussed below.

5. DISCUSSION

The results of present analysis are in general agreement with some experimental data reported in the literature, but at odds with other published data. In particular, Bradley (1989) presented his experimental results for the ratio of mode II delamination toughness to mode I delamination toughness for a variety of resin adhesives. The ratio Γ_{IIc}/Γ_{Ic} for the brittle resins varies from 3 to 11, with most data in the range from 3 to 6. It should be expected that the present theoretical results should tend to bound the experimental data from below for two reasons. Firstly, the response of the adhesive has been assumed to be purely elastic with no accounting for plasticity, and plasticity is expected to have more effect on the mode II toughness than the mode I toughness. Secondly, it has been assumed that there exists an ample population of initial flaws whose size is comparable to the thickness of the brittle adhesive layer. It is from these flaws that the tunnel cracks spread. If the population of initial flaws was of a size significantly smaller than the layer thickness (e.g., on the order of $H/5$), then larger applied stresses would be necessary to initiate the tunnel cracks than is predicted by the steady-state tunneling analysis. The tunneling process would then involve the dynamic propagation of the microcracks and the dissipation of more energy than is predicted by the present quasi-static analysis. Assuming the microcracking process is brittle, we interpret the existence of experimentally measured ratios of Γ_{IIc}/Γ_{Ic} well in excess of three to be indirect evidence of the fact that those adhesives have initial flaws which are small compared to the layer thickness.

The present results for the mode II toughness are independent of the layer thickness $2H$ and do not depend explicitly on any details of the initial flaw population. In this sense the present results are similar to Fleck's result which is independent of the spacing of the periodically distributed echelon cracks. In the present modeling, this independence is a consequence of the assumption of an ample population of relatively large flaws. If, instead, there existed an ample population of small flaws, then one would expect the size of the flaws to enter into the dependence of Γ_{IIc}, primarily because an over-stress will be needed to initiate the tunnel cracking process. On the other hand, if the flaw population were sparse and widely spaced compared to the layer thickness, then one would expect the layer thickness as well as the spacing and, possibly, the size of the flaws to influence Γ_{IIc}. In either case, Γ_{IIc} is expected to exceed the three or four times Γ_{Ic} predicted by the present analysis.

Qualitative features of the macroscopic mode II fracture behavior are also seen in the experimental results on a brittle adhesive (H3502) reported by Chai (1988), especially the mode I character of the microscopic cracking within the layer. However, Chai's observations differ from the theoretical predictions in several significant respects. He observes a strong dependence of the macroscopic mode II toughness on the adhesive layer thickness with Γ_{IIc}/Γ_{Ic} about three for small thicknesses increasing to more than 20 at larger thicknesses between 10 and 50 μm. Moreover, the experimentally observed microcrack density in the failed layer was typically an order of magnitude lower than the theory would suggest. Whether these discrepancies are due to plasticity, interface failure due to low interface toughness, or the small initial flaw population just discussed is not known. It is evident from Chai's (1988) paper that the relationship between macroscopic mode II toughness of a joint and the thickness of the adhesive layer is not nearly as simple as the present model predicts. Further work will be required before a complete theory is in hand.

Two constraint limiting constraint conditions have been considered leading to the two sets of predictions presented above. In addition, to simplify the analysis and to reduce the number of parameters in the problem, the compliance of the adjoining solids has been neglected compared to that of the adhesive. This is probably a reasonable approximation for many systems based on polymeric adhesives. For such systems, it would also seem that the second constraint assumption of zero normal displacement to the layer would be the more reasonable one, but that may depend on the details of the test specimen geometry. The main conclusion to be drawn from the results for the two limiting constraints is that there is not an unduly large difference in the resulting predictions.

Acknowledgements—This work was supported in part by the DARPA University Research Initiative (Subagreement P.O. #KK3007 with the University of California, Santa Barbara, ONR Prime Contract N00014-92-J-1808), by the National Science Foundation Grant NSF-MSS-92-02141, and by the Division of Applied Sciences, Harvard University.

REFERENCES

Ashby, M. F. and Hallam, B. D. (1986). The failure of brittle solids containing small cracks under compressive stress states. *Acta Metall.* **34,** 497–510.

Beuth, J. L. (1992). Cracking of thin bonded films in residual tension. *Int. J. Solids Structures* **29,** 1657–1675.

Bradley, W. L. (1989). Relationship of matrix toughness to interlaminar fracture toughness. In *Application of Fracture Mechanics to Composite Materials* (Edited by K. Friedrich), pp. 159–186. Elsevier.

Chai, H. (1988). Shear fracture. *Int. J. Fracture* **37,** 137–159.

Fleck, N. A. (1991). Brittle fracture due to an array of microcracks. *Proc. R. Soc.* **A432,** 55–76.

Fleck, N. A. (1992). Private communication.

Fleck, N. A., Hutchinson, J. W. and Suo, Z. (1991). Crack path selection in a brittle adhesive layer. *Int. J. Solids Structures* **27,** 1683–1703.

Freund, L. B. and Kim, K. S. (1991). Spiral cracking around a strained cylindrical inclusion in a brittle material and implications for vias in integrated circuits. In *Mechanical Behavior of Materials and Structures in Microelectronics* (Edited by Z. Suhir, R. C. Cammarata and D. D. L. Chung), Vol. 226, pp. 291–302. MRS.

Hibbs, M. F. and Bradley, W. L. (1987). Correlations between micromechanical failure processes and the delamination toughness of graphite/epoxy systems. In *Fractography of Modern Engineering Materials* (Edited by J. E. Masters and J. Au), STP 948, pp. 68–97.

Ho, S. and Suo, Z. (1993). Tunneling cracks in constrained layers. *J. Appl. Mech.* **60,** 890–894.

Horii, H. and Nemat-Nasser, S. (1986). Brittle failure in compression: splitting, faulting and brittle-ductile transition. *Phil. Trans. R. Soc.* **A319,** 337–374.

Hutchinson, J. W. and Suo, Z. (1991). Mixed mode cracking in layered materials. In *Advances in Applied Mechanics* (Edited by J. W. Hutchinson and T. Y. Wu), Vol. 28, pp. 63–191. Academic Press, New York.

Nakamura, T. and Kamath, S. M. (1992). Three-dimensional effects in thin film fracture mechanics. *Mech. Mater.* **13,** 67–77.
Ortiz, M. (1988). Microcrack coalescence and macroscopic crack growth initiation in brittle solids. *Int. J. Solids Structures* **24,** 231–250.
Rice, J. R. (1968). Mathematical analysis in the mechanics of fracture. In *Fracture, An Advanced Treatise* (Edited by H. Liebowitz), Vol. II, pp. 191–311. Academic Press, New York.
Smith, B. W. and Grove, R. A. (1987). Determination of crack propagation directions in graphite/epoxy structures. In *Fractography of Modern Engineering Materials* (Edited by J. E. Masters and J. Au), STP **948,** pp. 154–173.
Tvergaard, V., Xia, Z. C. and Hutchinson, J. W. (1993). Cracking due to localized hot shock. *J. Am. Ceram. Soc.* **76,** 729–736.
Ye, T., Suo, Z. and Evans, A. G. (1992). Thin film cracking and the role of substrate and interface. *Int. J. Solids Structures* **29,** 2639–2648.

APPENDIX. AN ARRAY OF DISLOCATIONS IN A BRITTLE ADHESIVE LAYER

The dislocation solution used to solve the plane strain problem is outlined here.

The plane strain elasticity problem is specified in Fig. A1(a). An array of edge dislocations with Burger's vector $\mathbf{b} = (b_x, b_y)$ lies along the x-axis with uniform spacing π. The upper boundary lies along $y = d$ and the lower boundary along $y = -c$. The elastic material has shear modulus, μ, and Poisson's ratio ν. The thickness of the layer is $c+d = 2H$. The boundaries are considered to be rigid. The elastic solution to this problem is obtained by superimposing the solutions to the following two problems: (a) an array of same dislocations lies in an infinite elastic body; and (b) a dislocation-free strip of thickness $2H$, with prescribed displacements along both upper and lower boundaries. The displacements are chosen to cancel that calculated from problem (a).

Problem (a)

The solution to this problem is given by the Muskhelishvili potentials

$$\phi(z) = A \ln(\sin z), \qquad \Omega(z) = \bar{A} \ln(\sin z) \tag{A1}$$

where

$$z \equiv x+\mathrm{i}y, \qquad A = \frac{\mu(b_y - \mathrm{i}b_x)}{4\pi(1-\nu)}.$$

The stresses and displacements are given by

$$\sigma_x + \sigma_y = 2[\phi'(z) + \overline{\phi'(z)}] \tag{A2}$$

$$\sigma_y - \sigma_x + 2\mathrm{i}\sigma_{xy} = 2[(\bar{z}-z)\phi''(z) + \Omega'(z) - \phi'(z)] \tag{A3}$$

and

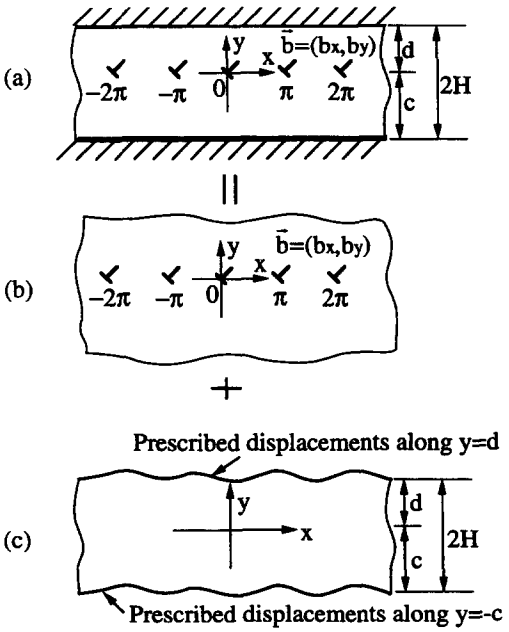

Fig. A1. Stress distribution solution by a superposition scheme. (a) An array of dislocations in an elastic strip. (b) An array of dislocations in an infinite elastic body. (c) A dislocation-free strip with prescribed displacements along edges.

$$2\mu(u_x+u_y)=(3-4\nu)\phi(z)+(\bar{z}-z)\overline{\phi'}(z)-\overline{\Omega}(z). \tag{A4}$$

The displacement along $y=d$ and $y=-c$ are periodic functions and thus can be expressed in terms of Fourier sine and cosine series.

Problem (b)

Consider a dislocation-free strip with prescribed displacements along boundaries as shown in Fig. A1(c). Following Fleck (1991), we introduce two real potentials $U(x, y)$ and $X(x, y)$ satisfying

$$\nabla^4 U(x,y)=0, \qquad \nabla^2 X(x,y)=0, \qquad \frac{\partial^2 X(x,y)}{\partial x\partial y}=\tfrac{1}{4}\nabla^2 U(x,y). \tag{A5}$$

The stresses and displacements can be derived from

$$\sigma_x=\frac{\partial^2 U}{\partial y^2}, \qquad \sigma_y=\frac{\partial^2 U}{\partial x^2}, \qquad \sigma_{xy}=-\frac{\partial^2 U}{\partial x\partial y} \tag{A6}$$

$$2\mu u_x=-\frac{\partial U}{\partial x}+4(1-\nu)\frac{\partial X}{\partial y}, \qquad 2\mu u_y=-\frac{\partial U}{\partial y}+4(1-\nu)\frac{\partial X}{\partial x}. \tag{A7}$$

The general procedure is to represent $U(x, y)$, $X(x, y)$ as Fourier series in x. Solutions of these two potentials can be derived by canceling the displacements u_x and u_y along boundaries $y=a$ and $y=-c$ obtained from (A4). The details of solution procedure are omitted here. Helpful hints can be found in Fleck (1991).